Available online at www.sciencedirect.com

ScienceDirect

Geochimica et Cosmochimica Acta 333 (2022) 362–372

Geochimica et Cosmochimica Acta

www.elsevier.com/locate/gca

# The influence of sediment diagenesis and aluminium on oxygen isotope exchange of diatom frustules

Shaun P. Akse, Lubos Polerecky, Michiel V.M. Kienhuis, Jack J. Middelburg *

*Department of Earth Sciences, Utrecht University, PO Box 80021, 3508 TA Utrecht, the Netherlands*

Received 30 January 2021; accepted in revised form 13 July 2022; available online 19 July 2022

**Abstract**

The oxygen isotope composition of diatom frustules, $\delta^{18}O_{diatom}$, is thought to reflect the isotopic composition of the ambient seawater at the time of biomineralization. However, the $\delta^{18}O_{diatom}$ can be overprinted due to the susceptibility of silanol groups (both external and internal) to isotope exchange. Here, using high-resolution imaging, we investigate what factors may influence this post-mortem isotopic alteration during the initial stages of diagenesis in the sediment. A diatomaceous clay was incubated with $^{18}O$-enriched seawater with fresh diatom detritus placed at the sediment–water interface (SWI) and at depth in the sediment. NanoSIMS analysis showed that the fresh diatom detritus as well as fossil frustules became significantly enriched in $^{18}O$, and that a relationship between Al-content and $^{18}O$-exchange could be observed. To further study the potential role of Al as an inhibitor of oxygen exchange, we measured Al on the surface of fossil frustules and performed additional incubations of diatom detritus in seawater with various concentrations of dissolved Al. The presence of Al-rich material bound to the surface of fossil frustules did not reduce the extent of $^{18}O$-enrichment in the underlying silica. However, exposure of diatoms detritus to dissolved Al, which led to a significant increase in frustule Al/Si ratio and a homogenously distributed Al in the frustule valve, significantly lowered the amount of $^{18}O$-enrichment. We hypothesize that Al incorporated into the silica structure can slow down $^{18}O$ exchange while Al present as surface contaminants (clays or other aluminosilicates) has no inhibitory role.



*Keywords:* Diatom frustule; Oxygen; Isotope exchange; Maturation; Aluminium; NanoSIMS

## 1. INTRODUCTION

Studying changes in the oxygen isotope composition of various carbonate and silica remains is a common tool in paleoceanography, as these changes are thought to reflect changes in the temperature and isotope composition of the water in which they were formed (e.g., Rohling and Cooke, 1999; Zachos et al., 2001; Swann and Leng, 2009). Traditionally, the focus has been on foraminiferal carbonates, but diatomaceous silica has been receiving increasing attention over the last few decades. Oxygen isotope analysis of diatom silica has been performed in both marine and lacustrine settings (Labeyrie, 1974; Labeyrie and Juillet, 1982; see the reviews by Leng and Barker, 2006; Swann and Leng, 2009). However, despite increasing interest, the mechanisms through which changes in diatom silica oxygen isotopes relate to environmental change remain poorly understood. This is, in part, due to persisting concerns about possible diagenetic overprinting (DeMaster, 2002).

Concerns surrounding diagenetic influences exist due to the nature of the amorphous silica structure. While the structure of diatom frustules is composed predominantly of interlinked silica ($SiO_4$) tetrahedrons, a less dense hydrous layer consisting of loosely bonded -Si-OH molecules (silanol groups) surrounds the $SiO_4$ silica

* Corresponding author.
*E-mail address:* J.B.M.Middelburg@uu.nl (J.J. Middelburg).

https://doi.org/10.1016/j.gca.2022.07.015
0016-7037/

(Gendron-Badou et al., 2003). Silanols can be present on the surface of the frustule (external) or trapped in the porous structure as internal silanols (Loucaides et al., 2010; Zhuravlev, 2000). This poses a problem for the $\delta^{18}O_{diatom}$ proxy as the oxygen in the -Si-OH molecules is known to rapidly exchange with oxygen molecules in the surrounding water (e.g., Labeyrie and Juillet, 1982; Knauth and Epstein, 1982; Smith et al., 2016; Menicucci et al., 2017; Tyler et al., 2017; Dodd et al., 2012; Ryves et al., 2020; Akse et al., 2020 amongst others). Despite the development of various methods to account for or remove the exchangeable oxygen such as the controlled isotope exchange method (Labeyrie and Juillet, 1982; Juillet-Leclerc and Labeyrie, 1987) and the stepwise fluorination methods (Matheney and Knauth, 1989; Leng and Sloane, 2008) (see Chapligin et al., 2011 for a comparative study), the measured oxygen isotope composition is still thought to represent a combination of signals. This includes the formation signal but also post-mortem signals obtained during time spent in the water-column and sediment, and during laboratory processing. These concerns can be found for example in the observed differences in $\delta^{18}O_{diatom}$ between surface-water diatoms and diatoms taken from deep-water traps and surface sediments (Schmidt et al., 2001). Secondary oxygen exchange may also explain the variability found in calculated silica-water fractionation factors (fresh/recent diatom frustules: Brandriss et al., 1998; Moschen et al., 2005; Dodd and Sharp 2010; Ryves et al., 2020; sedimentary diatomaceous silica: e.g., Juillet-Leclerc and Labeyrie 1987; Matheney and Knauth, 1989; Shemesh et al., 1992).

Studies of post-mortem diagenesis have suggested several active processes that may influence $\delta^{18}O_{diatom}$. These include post-depositional partial dissolution (Smith et al. 2016; Ryves et al., 2020), the precipitation of secondary silica and addition of silanol groups, and the condensation of silanol groups to siloxane (Schmidt et al., 2001; Dodd et al., 2012, 2017; Moschen et al., 2006, Rickert et al., 2002; Loucaides et al., 2010). A result of these diagenetic processes is the decreasing reactivity of the frustules during maturation (Lewin, 1961). Silica condensation and subsequent reduction in silanol abundance has been suggested to be a main contributor to the observed decreasing reactivity, a process that is suggested to continue for about $10^4$–$10^6$ years (Dodd et al., 2017). This means that isotopic re-equilibration of oxygen in diatom frustules could continue on geological time-scales.

Based on this research, it appears that the amount of available reactive sites (e.g., silanol groups) is a predominant factor controlling oxygen exchange. Next to the proposed maturation processes, studies have shown that the incorporation of metals during diatom growth, post-mortem or diagenesis can also strongly reduce the reactivity of frustules. In particular the presence and incorporation of aluminium (Al) in the silica structure has been linked to reduced reactivity and solubility (Van Bennekom et al., 1991; Dixit et al., 2001). This incorporation is driven by the presence of the reactive silanol groups, which are excellent ligands for metals (Dixit and Van Cappellen, 2002). The Al taken up during secondary processes has been shown to originate from detrital materials and can become structurally incorporated into the silica framework by forming a new surface phase on the frustule (aluminosilicate coating) or by altering the existing mineral structure by replacing Si atoms (van Cappellen and Qiu, 1997; Dixit et al., 2001; Koning et al., 2007; Ren et al., 2013; Michalopoulos and Aller, 2004). The resulting deposition and incorporation of Al appears to take place on the timescales of mere days to weeks (Koning et al., 2007; Hendry et al., 2010). The formation of aluminosilicates can result in a negative charge, which repels the hydroxyl ions responsible for silica dissolution (Iler, 1973, 1979), thus protecting the frustule from dissolution and possibly also from secondary oxygen entering the structure.

Recently, using high-resolution isotope mapping it was confirmed that partial overprinting of the $\delta^{18}O$ signal in diatom frustules can already take place on timescales of days to weeks (Akse et al., 2020). Such overprinting was observed not only in diatom frustules but also in siliceous sponge spicules, which is another form of biogenic amorphous silica. Furthermore, it was shown that the external and internal silanol pools are similarly susceptible to partial overprinting on short timescales. This results in the presence of a large internal oxygen pool directly influenced by changes in the external water signature over multiple timescales (Menicucci et al, 2017; Dodd et al., 2017). This is of importance as earlier research has suggested that the condensation of internal silanols can occur to form siloxane during maturation (Schmidt et al., 2001; Dodd et al., 2012, 2017; Moschen et al., 2006) or laboratory treatment (Tyler et al., 2017). The post-mortem siloxane is likely not (fully) removed with current dehydroxylation techniques as these focus on the freely exchangeable oxygen. Therefore, an incorporation of this signal during maturation suggests that the final $\delta^{18}O$ signal of fossil biogenic silica represents a mixture of different signals including the original surface water signal, the signal from the water column during sinking, the signal from the sediment–water interface and artefacts from laboratory treatments.

This study investigates alteration of the $\delta^{18}O$ signal in diatom frustules during early diagenesis including residence at the sediment–water interface, after burial and after maturation in the sediment. First, fresh diatom detritus packed into folded polycarbonate filters was placed on top of, and in, a siliceous ooze, followed by the addition of natural or $^{18}O$-enriched seawater under anoxic conditions. After two weeks of incubation, $\delta^{18}O$ in individual frustules from these packets as well as in fossil frustules from the surrounding sediment were analysed by nanoSIMS. The results showed that $^{18}O$ exchange occurred in all samples, but the rate decreased with increasing maturation stage. To elucidate whether this trend could be due to metal incorporation, we subsequently incubated cultured diatom frustule detritus in $^{18}O$-label natural seawater containing various concentrations of dissolved aluminium and analysed their $^{18}O$-enrichment along with Al content with nanoSIMS. The results showed that the incorporation of Al slowed down secondary $^{18}O$-exchange whereas the presence of surface contaminations (clays or other aluminosilicates deposits) had no effect.

## 2. MATERIALS & METHODS

### 2.1. Materials

Two separate diatom batches were cultured (*Thalassiosira pseudonana* and *Thalassiosira weisflogii*) at the Royal Netherlands Institute for Sea Research (NIOZ) by using an f/2 medium based on natural seawater (NSW). The *T. weisflogii* strain (CCAP 1085/18) was provided by the culture collection of the NIOZ while the *T. pseudonana* strain (CCAP 1085/12) was acquired at the Culture Collection of Algae and Protozoans (CCAP). Cultures were grown in 300 $cm^3$ tissue culture flasks at a temperature of 20 °C under a 16 h/8h light/dark cycle. A total of 2 L of medium per diatom species was produced and split into 500 mL containers for harvesting. After harvesting the frustules were freeze-dried (Telstar LyoQuest) and stored at −20 °C. An aliquot of each 500 mL container was taken for cell count determination using flow cytometry. Frustule diameters ranged between 4 and 10 µm.

The diatomaceous clay sediment used in this study was provided by Henko de Stigter (NIOZ). It was originally collected in the Peru basin (07°04.4′ S, 088°27.8′ W) at 4150 m water depth during the summer of 2015. The sediment was the remainder of a boxcore after the top 20 cm had been removed; we thus estimate that the fossil frustules have an age of more than 10,000 years (Akse, 2020). After collection, the sediment was stored at 5 °C.

### 2.2. Incubation experiment in sediment with $^{18}$O-enriched porewater

Incubations took place in an anoxic glovebox located in a temperature-controlled room (20 °C). Natural seawater (NSW) and diatomaceous sediment were placed in the anoxic glovebox for 24 h and subsequently mixed at a 1:1 vol ratio. Freeze-dried pellets of cultured diatoms were diluted with 50 mL of MilliQ (18.2 MΩ· cm at 25 °C), and 0.1 mL of this solution was pipetted onto a polycarbonate (PC) filter (3 µm pore size, Nuclepore). The filters were then folded several times to enclose the diatom frustules in a packet. For each incubation, a 1.5 mL Eppendorf vial was filled with 0.25 mL of the sediment–water mixture. One of the filter packets was then placed in the tube and topped with another 0.25 mL of the sediment–water mixture, placing the packet at a depth of ~ 1 cm. After another diatom packet was placed on top of the sediment surface, the tube was topped with $^{18}$O-enriched NSW ($^{18}$O atom fraction of 9 %) prepared by mixing 1 mL of NSW with 0.1 mL of 97 % $H_2^{18}O$ (Sigma-Aldrich). It was estimated that it took three days for the $^{18}$O-enriched water to diffuse through the sediment. The tightly closed vials were placed in an upright position in a water bath (to further minimize temperature fluctuations) and incubated for 336 h. Incubations were terminated by removing vials from the glovebox and isolating the filters. Using a filtration set-up, the contents of the filters were rinsed onto clean PC filters (0.2 µm pore size, Nuclepore) and left to dry in air (see Tyler et al., 2017 for a study on the effects of drying and storage on diatom $\delta^{18}O$). Finally, the remaining sediment was washed and sieved (100, 60 & 40 µm sieves). The 40–60 µm size fraction was dried in a Petri dish and stored for later analysis while the other fractions were discarded.

### 2.3. Incubation experiment in $^{18}$O-enriched seawater with added dissolved Al

This experiment was performed in $^{18}$O-enriched NSW ($^{18}$O atom fraction of 9 %, see above) to which dissolved Al was added to obtain final concentrations of 0, 150 nM and 500 nM above the background. This is in the range of observed pore-water Al concentrations (Mackin and Aller, 1984). The solutions were prepared by mixing the appropriate amounts of NSW and an Al stock solution (10032 ± 32 µg aluminium $mL^{-1}$, 99.9981 % material purity, 7 % $HNO_3$ matrix; Inorganic ventures). One mL of each solution was added to a separate 1.5 mL Eppendorf tube, followed by the addition of the previously prepared diatom detritus (mixture of *T.pseudonana* & *T.weisflogii*; see above) in 0.01 mL aliquots. Subsequently, the Eppendorf tubes were put into Greiner tubes, placed in a horizontal position on a roller-table to keep the water moving and the material in suspension, and incubated for 168 h in a climate-controlled room (15 °C). At the end of the incubation, the samples were centrifuged for 10 min (RCF = 15411 g, 20 °C), the material was rinsed with MilliQ and filtered onto a PC filter (0.2 µm pore size). The filter was then air-dried and stored for later analysis in a Petri dish at 15 °C.

### 2.4. Sample preparation and NanoSIMS imaging

To prepare the samples for nanoSIMS analysis, dried PC filters with the diatom detritus were coated with a 12 nm Au-layer using a sputter coater (JOEL JFC-2300HR high-resolution fine coater, JEOL FC-TM20 thickness controller). The frustules received no additional treatment prior or after this step. The samples were then imaged with table-top SEM (JEOL JCM-6000PLUS NeoScope Benchtop SEM) operating at a 10-kV accelerating voltage for target identification.

Nanoscale secondary ion mass spectrometry was performed with the nanoSIMS 50L instrument (Cameca) operated at Utrecht University (see Nuñez et al. (2018) for a review of the method). Electron multiplier detectors were set using a standard (SPI Supplies, 02757-AB 59 Metals & Minerals Standard) to enable the detection of secondary ions $^{12}C^-$, $^{16}O^-$, $^{18}O^-$, $^{12}C^{14}N^-$, $^{28}Si^-$ and $^{27}Al^{16}O^-$ with the $Cs^+$ primary ion beam. While $^{16}O^-$, $^{18}O^-$, $^{28}Si^-$ and $^{27}Al^{16}O^-$ ions are the focus of this study, $^{12}C^-$ and $^{12}C^{14}N^-$ ions were used to identify the background filter and any remaining organic matter on the frustules. First, samples were placed in the airlock to reach vacuum levels of $10^{-8}$ mbar and heated to about 50 °C for at least 24 h to remove any adsorbed water. Subsequently, the samples were moved to the vessel chamber and kept in a vacuum ($10^{-9}$ mbar; 20 °C) for at least 3 days until analysis.

For the diatom detritus samples, low-energy implantation was used to implant $Cs^+$ ions into the surface of the frustules for better secondary ion yields without eroding

the material of the sample. To reach stable secondary ion yields from the fossil frustules, the measurement area was pre-sputtered with the primary ion beam (FCo current 20 pA). Pre-sputtering diaphragm settings were first set to D1-0, with C4y set to 50 bits to avoid detector overloading, and the pre-sputtering was monitored until the counts at detector #3 ($^{28}Si^-$) reached about 170 kcps. This was followed by the diaphragm switched to D1-1 until stable secondary ion counts were reached. After pre-sputtering, analysis was carried out in the imaging mode by rastering a high-energy $Cs^+$ beam (16 keV, current at the sample surface of 0.5 pA, nominal beam size 50–150 nm) over a targeted area on the frustule (between 7 × 7 μm and 20 × 20 μm in size) and measuring the sputtered secondary ions at a resolution of 128 × 128 pixels and with a dwell time of 1 ms/pixel. The diaphragm and slit settings were D1-3, ES-3, AS-2, EnS-1. Analysis generally continued until the integrity of the frustules was lost as observed by strong mutations to the physical structure.

### 2.5. NanoSIMS data processing

NanoSIMS data were analysed with an updated version of the Matlab-based software Look@NanoSIMS (Polerecky et al., 2012). The general approach involved the analysis of ion count ratios in manually drawn regions of interest (ROIs), and their variations with depth (measurement plane) in the sample. The ROI-specific $^{18}O$ atom fraction, x($^{18}O$), was calculated from the secondary ion counts accumulated over the ROI pixels as $^{18}O/(^{16}O+^{18}O)$. The negligible contribution of the isotope $^{17}O$ was not considered.

Depth profiles measured in fresh frustules showed an increase in the x($^{18}O$) and a decrease in the $^{27}Al^{16}O^-/^{28}Si^-$ ion count ratios during the first 50–200 planes (Supplementary Fig. S1). The initial increase in the $^{18}O$ atom fraction was attributed to sample preparation (rinsing with MilliQ), whereas the decrease in the $^{27}Al^{16}O^-/^{28}Si^-$ ion count ratio was likely due to secondary ion yields not being completely stable after the initial low-energy implantation step of the measurement (see additional details in Fig. S1). For the final dataset in Fig. 4, the initial 50–200 planes were therefore disregarded, and the data-points represent the mean and standard error over the planes where the ratios were stable. Furthermore, only the frustule valves, not the frustule girdle bands, were considered as these are commonly studied in the sedimentary archive.

Similar variation with depth was observed in fossil frustules for the $^{27}Al^{16}O^-/^{28}Si^-$ ion count ratios but not for the $^{18}O$ atom fractions (Fig. S2). In contrast to fresh frustules, the fossil frustules were thoroughly pre-sputtered before each measurement, which was expected to stabilize the secondary ion yields (see Section 2.4). Thus, it is likely that the observed decline in the $^{27}Al^{16}O^-/^{28}Si^-$ ion count ratio represented true variation of Al/Si with depth in the silica frustule. The final dataset in Fig. 3 therefore shows statistics obtained from all planes measured in the individual frustules. Specifically, the data-points correspond to the median, while the error bars indicate the range between the 17–83 percentiles (i.e., encompassing 66 % of values) divided by $\sqrt{N}$, where N is the number of planes measured. The error bars therefore represent the uncertainty with which the frustule-specific $^{18}O$ atom fractions and Al/Si ratios were determined. Because the depth-variation in the $^{18}O$ atom fractions was only determined by the ion counts (Poisson statistics), the uncertainty is equal to the Poisson error, i.e., the analytical precision of the NanoSIMS measurement. In contrast, the uncertainty of the Al/Si determination was mostly due to the variation of the ion count ratio with depth while the Poisson error was negligible.

## 3. RESULTS

### 3.1. Post-mortem $^{18}O$-enrichment of diatom frustules in the sediment

Representative images of $^{18}O$ atom fractions in diatom frustules clearly show that frustules incubated in $^{18}O$-enriched seawater had a significantly higher $^{18}O$ atom fraction than the control frustules (Fig. 1). Thus, placement of the frustules at or in the sediment did not stop secondary O-exchange. The fresh frustules placed at the sediment–water interface (Fig. 1b) were more enriched than those buried in the sediment (Fig. 1c), but this difference may have been partly due to the different exposure to $^{18}O$-enriched water linked to limited diffusive transport of the labelled water through the sediment. Fossil frustules of the surrounding sediment showed the lowest $^{18}O$-enrichment (Fig. 1d). In all frustules the $^{18}O$ enrichment was homogeneously distributed across the valve. However, in the fresh diatom detritus frustules, where we could additionally observe the girdle (proteinaceous silica bands connecting the valves), the $^{18}O$ enrichment in the girdle was significantly lower than in the valve (Fig. 1b).

### 3.2. Presence and influence of clay and other aluminosilicate contaminants on fossil frustules

NanoSIMS measurements of fossil frustules revealed highly heterogeneous distribution of Al signals (measured as $^{27}Al^{16}O^-$) on the frustule surface. In the SEM images (Fig. 2a) the larger Al-rich areas (Fig. 2b) could be identified as particulate material blocking the pores or as pore narrowing. Thus, we attribute these Al-rich signals to surface-bound or pore-bound contamination, possibly clay particles or aluminosilicates.

The Al-rich contaminants did not appear to be enriched in $^{18}O$. Although pixels near the contaminants showed slightly higher $^{18}O$ atom fractions ($\sim 2.4 \times 10^{-3}$), this was likely the result of mixing of signals from the $^{18}O$-enriched silica and the $^{18}O$-unenriched surface contaminant (Fig. 2c,d). Importantly, the $^{18}O$ atom fraction in the Al-rich areas increased with the measurement plane (i.e., depth) and reached the same level as in the surrounding silica when the Al-rich contaminant was sputtered away (Fig. 2e,f). This shows that the surface-bound particulate contamination did not prevent the underlying silica matrix from becoming enriched in $^{18}O$ during the incubation.

To ensure that the silica-specific $^{18}O$ atom fractions and Al/Si ratios were not affected by the particulate con-

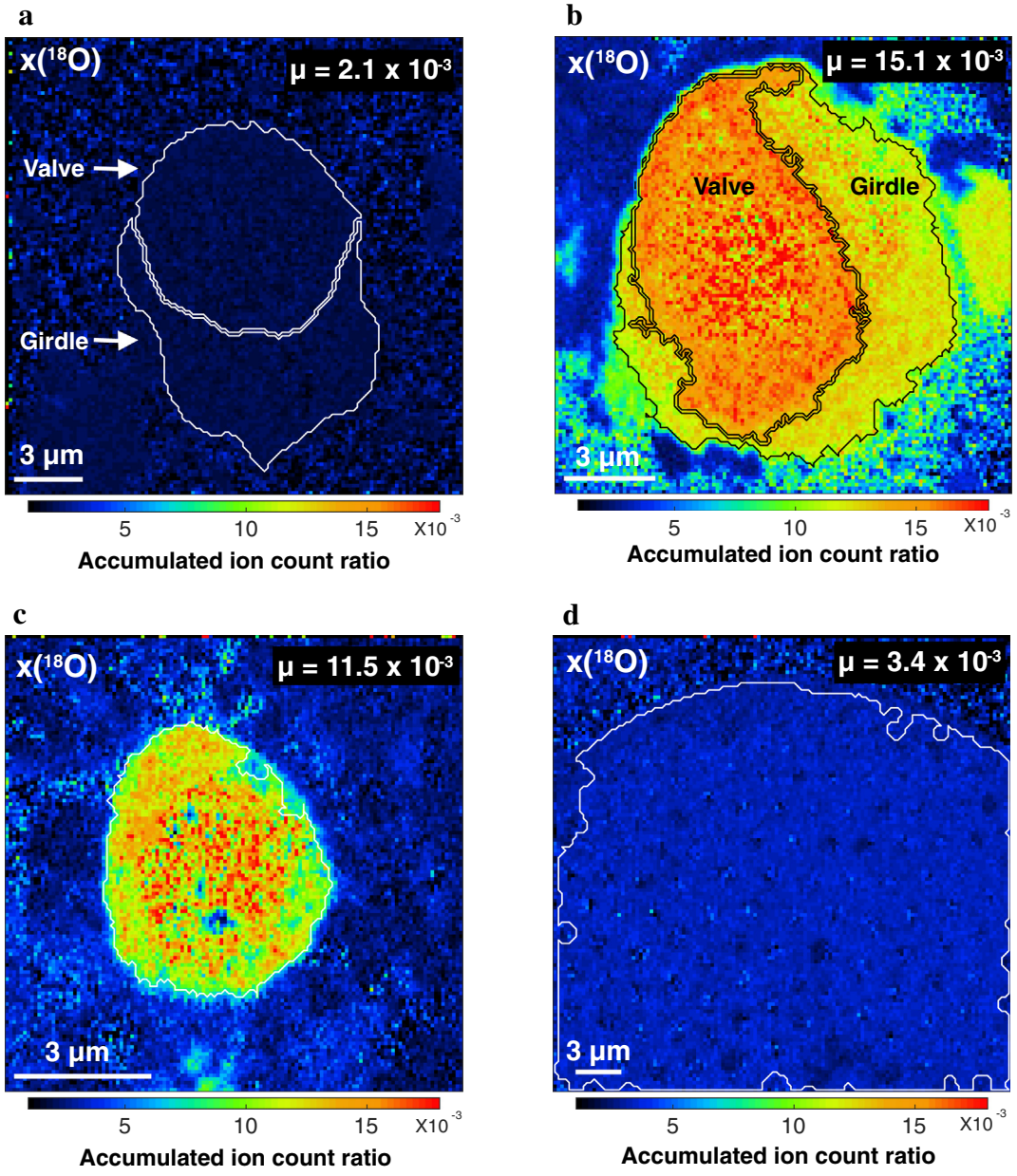


Fig. 1. **Imaging of $^{18}O$ atom fraction in diatom frustules incubated with $^{18}O$-enriched water.** Representative images are shown of **(a)** a fresh control frustule incubated in natural seawater, **(b)** fresh frustule placed at the sediment–water interface and incubated in $^{18}O$-enriched seawater, **(c)** fresh frustule placed at ~1 cm depth in the sediment and incubated in $^{18}O$ enriched seawater, and **(d)** a fossil frustule from the 40–60 μm size fraction of the surrounding sediment and incubated in $^{18}O$ enriched seawater. ROI outlines mark the frustule valve and girdle. SEM images of these samples are found in Fig. S3.

tamination, the Al-rich areas were excluded from the final analysis of fossil frustules. The results showed that the fossil frustules incubated in $^{18}O$-enriched seawater had significantly greater $^{18}O$ atom fractions than the control frustules (Fig. 3). The $^{18}O$ atom fractions and Al/Si ratios differed among individual frustules, but their correlation was not significant ($p = 0.602$; Table S1). The sediment incubated in $^{18}O$-enriched seawater contained some foraminiferal shells, and these were not enriched in $^{18}O$ (Fig. S4).

### 3.3. Influence of dissolved Al on $^{18}O$-enrichment in fresh frustules

The influence of Al-incorporation into the silica matrix on the rate of oxygen exchange between the frustule and seawater was studied in two ways. In the first approach, focusing on the impact of dissolved Al in the porewater (originating from the surrounding lithogenic particles), packets with fresh diatom detritus were placed at the sediment–water interface and at 1 cm depth in sediment and

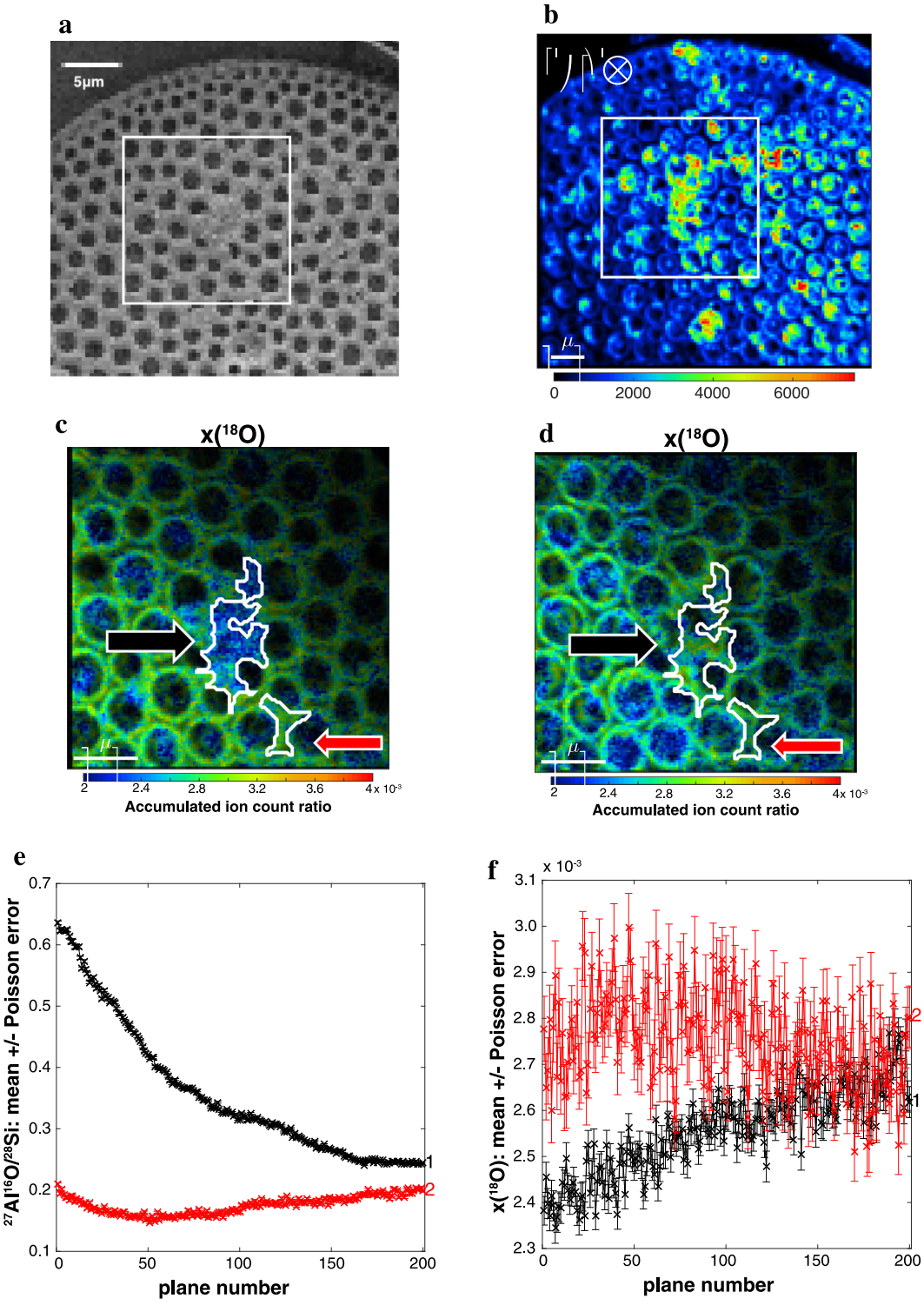


Fig. 2. **The presence and removal of Al on a fossil diatom frustule incubated in an $^{18}$O-enriched seawater. (a, b)** SEM and $^{27}Al^{16}O^-$ ion count image with white square showing the field-of-view for c-d; **(c, d)** Ion count maps of the $^{18}$O atom fraction. The hue of the image was modulated by the $^{16}$O intensity image to suppress noise in the background (c) Planes 1–300; (d) Planes 1700–2000; Outlines mark the ROIs used for (e,f), the coloured arrows indicate the corresponding lines in (e,f); **(e, f)** Ratios are shown as a function of the measurement plane (i.e. depth) accumulated in blocks of 10 planes. The lines represent the Al-contaminant (black line) and the surrounding silica (red line) from (c,d). A decreasing Al/Si trend is observed for the black line as the contaminant is sputtered away. As the contaminant is sputtered away, the $^{18}$O atom fraction increases (black line) until the ratios are similar to the surrounding silica (red line). A very slight decline is observed in the $^{18}$O-enrichment of the silica, while a slow increase is observed in the $^{27}Al/^{28}Si$. Imaging showed that this pattern was present predominantly around the pores, suggesting that an Al-presence from the pores may be influencing the silica data as more of the frustule is sputtered away.

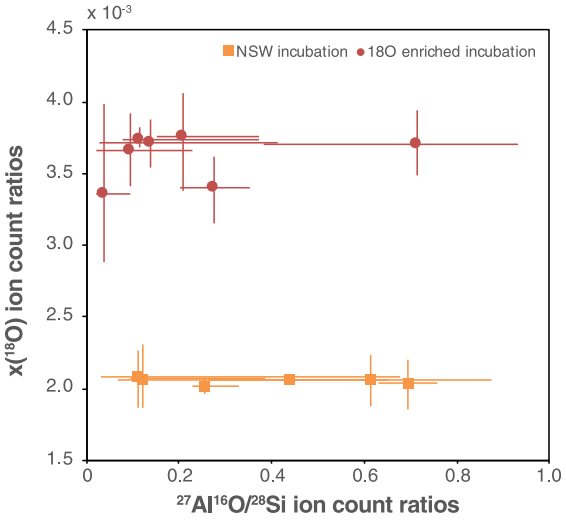


Fig. 3. **Graph showing $^{27}Al^{16}O/^{28}Si$ ion count ratios (a proxy for molar Al/Si ratio) vs $^{18}O$ atom fraction for fossil diatom frustules.** Each datapoint corresponds to an individual frustule. See Methods for the meaning of error-bars.

incubated in $^{18}O$-enriched seawater. Measurements of individual frustules revealed that the frustules at the sediment–water interface had significantly lower Al-content ($F = 24.7$; $p < 0.01$; Table S2, S3, S4) and significantly elevated $^{18}O$ atom fractions ($F = 23.0$; $p < 0.01$; Table S2, S3, S5) when compared with their counterparts that were buried in the sediment (Fig. 4a; Table 1).

In the second approach, fresh diatom detritus was incubated in the $^{18}O$-enriched natural seawater amended with dissolved Al (dAl; final concentrations of 0, 150, and 500 nM above background). The addition of dAl to the seawater was reflected in the Al/Si values of the frustules (Fig. 4b; Table 1), similar to results found in the literature (e.g., Koning et al., 2007). The addition of 500 nM dAl led to significantly higher $^{27}Al^{16}O/^{28}Si$ ion count ratios in the frustules compared to controls ($p < 0.05$; Table S6, S7, S8, S9). In the NanoSIMS images, Al appeared to be distributed rather homogenously through the frustule valve of these fresh materials (Fig. S1), in contrast to the high frequency hotspots observed in the fossil frustules (Fig. 2). The high dAl treatment also significantly lowered the $^{18}O$ atom fractions of the frustules compared to controls ($p < 0.05$; Table S6, S7, S10, S11). The addition of 150 nM also led to an increased Al-content and reduced $^{18}O$-enrichment in the frustules, but the differences relative to controls were not statistically significant (Tables S9 & S11).

In addition to differences between the mean values, the comparison of individual frustules from the two incubation experiments revealed significant negative correlations between the Al/Si ratios and the $^{18}O$ atom fractions (Fig. 4; $p < 0.05$; Table S12, S13, S14). The slopes of these correlations were not significantly different when comparing the incubations performed in the natural sediment and in the Al-enriched seawater (ANCOVA; $F_{interaction} = 0.714$; $p = 0.402$; Table S15), indicating similar mechanisms. Furthermore, the coefficient of determination was higher for the sediment experiment ($R^2 = 0.644$; Table S14) than the dAl experiment ($R^2 = 0.226$; Table S14).

## 4. DISCUSSION

Multiple studies have shown that oxygen isotope signature in biogenic silica is subject to secondary alteration (Labeyrie and Juillet, 1982; Schmidt et al., 2001; Moschen et al., 2006; Swann and Leng, 2009; Dodd et al., 2012,

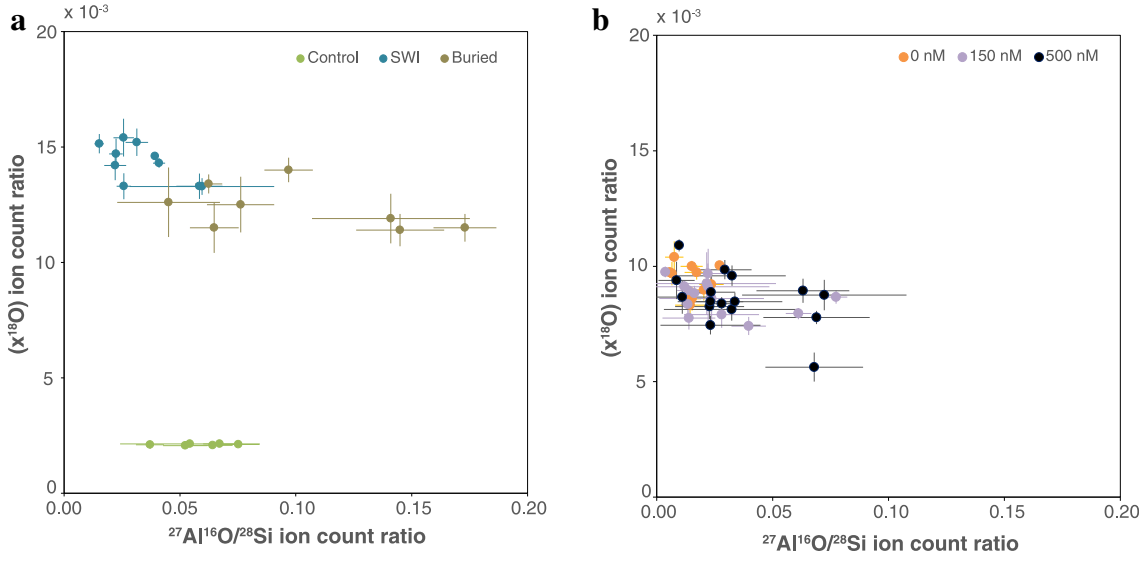


Fig. 4. **Silica-specific $^{27}Al^{16}O/28Si$ ion count ratios (a proxy for molar Al/Si ratio) vs $^{18}O$ atom fractions in fresh diatom frustules.** Data are shown from two incubation experiments in $^{18}O$-enriched seawater with error bars portraying standard deviation. **(a)** Frustules were placed at the sediment–water interface (SWI) or buried in the sediment for 2 weeks. The data for control frustules are also included. **(b)** Frustules were incubated for 1 week with different concentrations of dissolved Al (dAl).

Table 1
**Comparison of the chemistry of fresh diatom frustules incubated under different experimental settings.** Shown are the means of $^{27}Al^{16}O/^{28}Si$ ion count ratio (a proxy for molar Al/Si ratio) and $^{18}O$ atom fraction. The **'Sediment'** experiment compares the frustules placed at the sediment–water interface (SWI) and buried in the sediment for 2 weeks. The **'dAl'** experiment compares the frustules incubated for 1-week with different concentrations of dissolved Al (dAl).

| Experiment | | N | $^{27}Al^{16}O/^{28}Si \pm SD$ [$\times 10^{-2}$] | x($^{18}O$) $\pm$ SD [$\times 10^{-3}$] |
|---|---|---|---|---|
| 'Sediment' | SWI (Natural seawater) | 6 | 5.84 ± 1.34 | 2.11 ± 0.03 |
| | SWI ($^{18}O$-enriched seawater) | 10 | 3.41 ± 1.53 | 14.3 ± 0.81 |
| | Buried ($^{18}O$-enriched seawater) | 8 | 11.0 ± 4.67 | 12.4 ± 0.96 |
| 'dAl' | 0 nM | 11 | 1.51 ± 0.69 | 9.38 ± 0.69 |
| | 150 nM | 14 | 2.64 ± 2.03 | 8.66 ± 0.72 |
| | 500 nM | 16 | 3.44 ± 2.16 | 8.59 ± 1.15 |

2017; Smith et al., 2016; Menicucci et al., 2017; Tyler et al., 2017; Ryves et al., 2020; Akse et al., 2020 amongst others). Moreover, sample pre-treatments such as step-wise fluorination (Matheney and Knauth, 1989; Leng and Sloane, 2008) and controlled isotope exchange (Labeyrie and Juillet, 1982; Juillet-Leclerc and Labeyrie, 1987) may only partly remove the effects of post-mortem isotopic alteration of the silica (Dodd et al., 2017; Menicucci et al, 2017; Akse et al., 2020). In a previous study, we confirmed that biogenic silica undergoes a rapid resetting of the O-isotope signature when incubated in $^{18}O$-enriched seawater and the results suggested that external and internal silanol groups are similarly affected (Akse et al. 2020). This raised the question whether these post-mortem processes would continue when diatom detritus moves from the water column into the sediment, as studies have shown that the reactivity of the frustules decreases dramatically as a consequence of maturation during ageing (Dixit et al., 2001; Lewin, 1961 and others). In this study, we looked at oxygen exchange under various conditions representing the different stages of diagenesis and the role of dissolved Al as a potential inhibitor.

All the measured diatom frustules showed significant $^{18}O$ enrichment after having been incubated in $^{18}O$-enriched seawater for 336 h. Using high-resolution techniques, we confirmed that even in the sediments the oxygen signal of both fresh and fossil frustules can be quickly altered by the oxygen signal of the surrounding water. The strongest $^{18}O$ enrichment was observed in the frustules placed at the sediment–water interface. These generally also had a lower Al-content than their counterparts buried in the sediment. In addition to the study of fresh diatom detritus, fossil frustules from the surrounding diatomaceous pre-Holocene clay were also studied. Proof of frustule maturation is found in the higher Al-content when compared to the fresh frustules (Fig. S5; Gehlen et al., 2002; Van Cappellen et al., 2002; Moschen et al., 2006) and the lack of hydroxyl groups during Raman measurements (See Akse et al., 2020). Despite this more mature structure, the fossil frustules also showed an enrichment in $^{18}O$ albeit less strong than the fresh frustules.

As mentioned, decreasing $^{18}O$-enrichment is likely linked to increasing maturation. In this study, we studied whether this corresponded with Al-content of the frustule; a common marker for biogenic silica diagenesis (van Bennekom et al., 1991). The distribution of Al was different in the fossil frustules than the fresh frustules. In the valves of the fresh frustules, incubated in Al-enriched waters post-mortem, the increased Al-content was generally homogenously distributed (Fig. S1) whilst the fossil frustules showed an abundance of Al-hotspots (Fig. 2). The observed high Al-content in the frustules buried in the sediment is in correspondence with the literature. It has been shown that dissolved Al supply in the porewaters, originating from lithogenic particles, is higher than that in the water column (Mackin and Aller, 1984) and can be readily deposited on frustules post-mortem as aluminosilicates or can become structurally incorporated into the silica framework (van Cappellen and Qiu, 1997; Dixit et al., 2001; Koning et al., 2007; Ren et al., 2013; Michalopoulos and Aller, 2004).

Some of the larger Al-hotspots on the fossil frustules could be identified in the SEM image as a narrowing or blocking of the pores suggesting either clay or other aluminosilicate deposits. Detailed spatial analysis of these Al contaminants allowed us to sputter some of them away, exposing the silica underneath. The silica underneath this surface contaminant had identical $^{18}O$-enrichment as the other areas of the 'clean' silica structure, unlike the contaminant itself which did not display $^{18}O$-enrichment. These results show that aluminosilicate clay presence does not inhibit post-mortem alterations to the isotopic oxygen signature of diatom frustules. Moreover, these results show how the application of imaging techniques such as the nanoSIMS can be used to identify and eliminate small contributions of the contaminants that can have significant influences on the isotope values (Brewer et al., 2008).

The fresh diatom detritus showed a rather homogenous distribution of Al and $^{18}O$ through the frustule valves (Fig. S1). The lower Al-content and higher $^{18}O$ atom ratios of the frustules placed at the sediment–water interface relative to the buried frustules may be due to the higher availability of Al in the sediment and the diffusion gradient (estimated to last for about three days) of the $^{18}O$-enriched water into the sediment. However, it may also be that the reduced $^{18}O$-enrichment in the buried frustules confirms earlier observations that the transition of diatom detritus from the water column into the sediment results in decreasing reactivity due to interactions with metals in the pore water or differences in pH (Dodd et al., 2017, Rickert et al., 2002; Loucaides et al., 2010; Zhuravlev, 2000).

To further investigate the role of metals, an additional experiment was performed by placing frustules in $^{18}O$-enriched seawater with varying concentrations of

dissolved Al. In this approach, other potential contributing factors were removed and only the effect of Al was studied. As Al was homogenously distributed over the frustule valve, the increasing Al/Si with increasing dissolved Al most likely reflected the structural incorporation of Al (when a silicon atom is substituted by an Al(III) ion; Ren et al., 2013). Increasing the dissolved Al concentrations in the water resulted in significantly reduced $^{18}O$ atom fractions, suggesting an inhibitory role of diagenetically incorporated Al. The interaction between Al-content and $^{18}O$-enrichment was statistically the same among the sediment incubations and dissolved Al addition experiments, suggesting similar mechanisms. However, the low to moderate coefficients of determination between Al-content and $^{18}O$-enrichment suggest that the Al-content cannot be the only factor controlling the exchange of $^{18}O$. The presence of other metals, pore-water conditions and biogeochemical processes in the sediment should be studied to further understand the post-mortem development of $\delta^{18}O_{diatom}$.

## 5. CONCLUSIONS

Secondary alteration of oxygen isotope signals in biogenic silica over geological timescales have been well documented (Labeyrie and Juillet, 1982; Schmidt et al., 2001; Moschen et al., 2006; Swann and Leng, 2009; Dodd et al., 2012, 2017; Smith et al., 2016; Menicucci et al., 2017; Tyler et al., 2017; Ryves et al., 2020). Recently, Akse et al. (2020) confirmed that the oxygen signal in biogenic silica can be rapidly overprinted post-mortem, even during it's time sinking in the water column (Fig. 5). The study presented here sheds new light on how this process continues in the sediment. Diatom detritus placed at the sediment–water interface, buried in the sediment and the fossil frustules of the surrounding sediment all underwent significant $^{18}O$-enrichment but to varying degrees. A relationship was observed between increasing Al-content of the frustule and decreasing levels of $^{18}O$-enrichment. This relationship was further studied by incubating cultured diatoms post-mortem with varying levels of dissolved Al. The post-mortem incorporation of Al into the frustule structure limited $^{18}O$-exchange but the presence of surface contaminants (clays or other aluminosilicates) did not. Accordingly, changes in environmental conditions during diagenesis appear to reduce further $^{18}O$-exchange and thus contribute to the preservation of the isotope signals of diatoms.

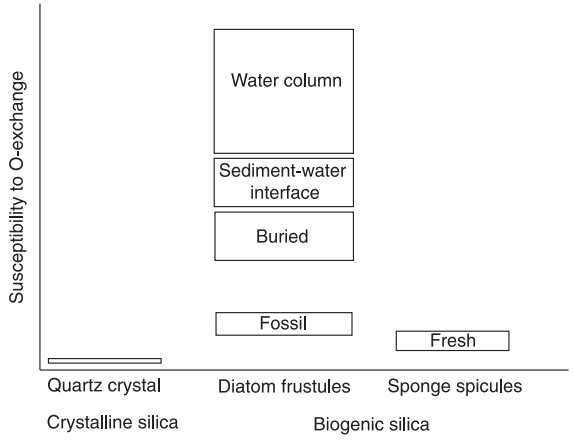


Fig. 5. **Conceptualization of the potential of different silica forms to become enriched in $^{18}O$** After being transported through the water column, diatom detritus will reach the sediment–water interface. Here the frustules will remain until they are buried and preserved over geological timescales. These processes lead to increasing maturity of the frustules and a decreasing susceptibility to secondary oxygen exchange. This figure is based on the results of this study as well as the results from previous research (Labeyrie and Juillet, 1982; Schmidt et al., 2001; Moschen et al., 2006; Swann and Leng, 2009; Smith et al., 2016; Menicucci et al., 2017; Tyler et al., 2017; Dodd et al., 2012, 2017; Ryves et al., 2020; Akse et al., 2020 amongst others).

## AUTHOR CONTRIBUTIONS

JJM, LP and SA designed the experiments. SA prepared the samples and conducted NanoSIMS analyses together with MK. SA and LP performed Nano- SIMS data analysis. SA interpreted the data, prepared the figures and wrote the manuscript text with contributions from all authors.

## DATA AVAILABILITY

The data presented in this study are available at https://doi.org/10.4121/13668950.

## DECLARATION OF COMPETING INTEREST

The authors declare that they have no known competing financial interests or personal relationships that could have appeared to influence the work reported in this paper.

## ACKNOWLEDGMENTS

We thank Dr. Kate Hendry and one anonymous referee for constructive feedback, M. Grego for culturing the diatom frustules and H. de Stigter for providing diatom ooze. The NanoSIMS facility at Utrecht University was financed through a large infrastructure grant by the Netherlands Organisation for Scientific Research (NWO) (grant no. 175.010.2009.011). This work was carried out under the programme of the Netherlands Earth System Science Centre (NESSC), financially supported by the Ministry of Education, Culture and Science (OCW) in the Netherlands (grant no. 024.002.001).

## APPENDIX A. SUPPLEMENTARY MATERIAL

Supplementary material to this article can be found online at https://doi.org/10.1016/j.gca.2022.07.015.

## REFERENCES

Akse S. P., Middelburg J. J., King H. E. and Polerecky L. (2020) Rapid post-mortem oxygen isotope exchange in biogenic silica. *Geochim. Cosmochim. Acta* **284**, 61–74.

Akse S. P. 2020. Studying climate signals through microscale chemical variability in diatoms: A high-resolution chemical imaging study of biogenic silica. Ph.D., thesis Utrecht University, ISBN: 978-90-6266-569-3.

Brandriss M. E., O'Neil J. R., Edlund M. B. and Stoermer E. F. (1998) Oxygen isotope fractionation between diatomaceous silica and water. *Geochim. Cosmochim. Acta* **62**, 1119–1125.

Brewer T. S., Leng M. J., Mackay A. W., Lamb A. L., Tyler J. J. and Marsh N. G. (2008) Unravelling contamination signals in biogenic silica oxygen isotope composition: the role of major and trace element geochemistry. *J. Quat. Sci.* **23**, 321–330.

Chapligin B., Leng M. J., Webb E., Alexandre A., Dodd J. P., Ijiri A., Lücke A., Shemesh A., Abelmann A., Herzschuh U., Longstaffe F. J., Meyer H., Moschen R., Okazaki Y., Rees N. H., Sharp Z. D., Sloane H. J., Sonzogni C., Swann G. E. A., Sylvestre F., Tyler J. J. and Yam R. (2011) Inter- laboratory comparison of oxygen isotope compositions from biogenic silica. *Geochim. Cosmochim. Acta* **75**, 7242–7256.

DeMaster D. J. (2002) The accumulation and cycling of biogenic silica in the Southern Ocean: Revisiting the marine silica budget. *Deep Res. PartII Top. Stud. Oceanogr.* **49**, 3155–3167.

Dixit Suvasi and Van Cappellen Philipp (2002) Surface chemistry and reactivity of biogenic silica. *Geochimica et Cosmochimica Acta* **66**(66), 2559–2568.

Dixit S., Van Cappellen P. and Van Bennekom A. J. (2001) Processes controlling solubility of biogenic silica and pore water build-up of silicic acid in marine sediments. *Mar. Chem.* **73**, 333–352.

Dodd J. P. and Sharp Z. D. (2010) A laser fluorination method for oxygen isotope analysis of biogenic silica and a new oxygen isotope calibration of modern diatoms in freshwater environments. *Geochim Cosmochim. Acta* **74**, 1381–1390.

Dodd J. P., Wiedenheft W. and Schwartz J. M. (2017) Dehydroxylation and diagenetic variations in diatom oxygen isotope values. *Geochim. Cosmochim. Acta* **199**, 185–195.

Dodd J. P., Sharp Z. D., Fawcett P. J., Brearley A. J. and McCubbin F. M. (2012) Rapid post-mortem maturation of diatom silica oxygen isotope values. *Geochem. Geophys. Geosyst.* **13**, 1–12.

Gehlen M., Beck L., Calas G., Flank A. M., Van Bennekom A. J. and Van Beusekom J. E. E. (2002) Unraveling the atomic structure of biogenic silica: Evidence of the structural association of Al and Si in diatom frustules. *Geochim. Cosmochim. Acta* **66**, 1601–1609.

Gendron-Badou A., Coradin T., Maquet J., Fröhlich F. and Livage J. (2003) Spectroscopic characterization of biogenic silica. *J. Non. Cryst. Solids* **316**, 331–337.

Hendry K. R., Meredith M. P., Measures C. I., Carson D. S. and Rickaby R. E. (2010) The role of sea ice formation in cycling of aluminium in northern Marguerite Bay, Antarctica. *Estuar. Coast. Shelf Sci.* **87**(1), 103–112.

Iler R. K. (1973) Effect of adsorbed alumina on the solubility of amorphous silica in water. *J. Colloid Interface Sci.* **43**, 399–408.

Iler R. K. (1979) *The chemistry of silica*. Wiley-Interscience, New York.

Knauth L. P. and Epstein S. (1982) The nature of water in hydrous silica. *Am. Mineral.* **67**, 510–520.

Koning E., Gehlen M., Flank A. M., Calas G. and Epping E. (2007) Rapid post-mortem incorporation of aluminum in diatom frustules: Evidence from chemical and structural analyses. *Mar. Chem.* **103**, 97–111.

Labeyrie L. (1974) New approach to surface seawater paleotemperatures using 18O/16O ratios in silica diatom frustules. *Nature* **248**, 40–42.

Labeyrie L. D. and Juillet A. (1982) Oxygen isotopic exchangeability of diatom valve silica; interpretation and consequences for paleoclimatic studies. *Geochim. Cosmochim. Acta* **46**, 967–975.

Leclerc A. J. and Labeyrie L. (1987) Temperature dependence of the oxygen isotopic fractionation between diatom silica and water. *Earth Planet. Sci. Lett.* **84**, 69–74.

Leng M. J. and Barker P. A. (2006) A review ofthe oxygen isotope composition oflacustrine diatom silica for palaeoclimate reconstruction. *Earth-Science Rev.* **75**, 5–27.

Leng M. J. and Sloane H. J. (2008) Combined oxygen and silicon isotope analysis of biogenic silica. *J. Quat. Sc.* **23**, 313–319.

Lewin J. C. (1961) The dissolution of silica from diatom walls. *Geochim. Cosmochim. Acta* **21**, 182–198.

Loucaides S., Behrends T. and Van Cappellen P. (2010) Reactivity of biogenic silica : Surface versus bulk charge density. *Geochim. Cosmochim. Acta* **74**, 517–530.

Mackin J. E. and Aller R. C. (1984) Diagenesis of dissolved aluminum in organic-rich estuarine sediments. *Geochim. Cosmochim. Acta* **48**, 299–313.

Matheney R. K. and Knauth L. P. (1989) Oxygen-isotope fractionation between marine biogenic silica and seawater. *Geochim. Cosmochim. Acta* **53**, 3207–3214.

Menicucci A. J., Spero H. J., Matthews J. and Parikh S. J. (2017) Influence of exchangeable oxygen on biogenic silica oxygen isotope data. *Chem. Geol.* **466**, 710–721.

Michalopoulos P. and Aller R. C. (2004) Early diagenesis of biogenic silica in the Amazon delta: Alteration, authigenic clay formation, and storage. *Geochim. Cosmochim. Acta* **68**, 1061–1085.

Moschen R., Lücke A. and Schleser G. H. (2005) Sensitivity of biogenic silica oxygen isotopes to changes in surface water temperature and palaeoclimatology. *Geophys. Res. Lett.* **32**, 1–4.

Moschen R., Lücke A., Parplies J., Radtke U. and Schleser G. H. (2006) Transfer and early diagenesis of biogenic silica oxygen isotope signals during settling and sedimentation of diatoms in a temperate freshwater lake (Lake Holzmaar, Germany). *Geochim. Cosmochim. Acta* **70**, 4367–4379.

Nuñez J., Renslow R., Cliff J. B. and Anderton C. R. (2018) NanoSIMS for biological applications: Current practices and analyses. *Biointerphases* **13**, 03B301.

Polerecky L., Adam B., Milucka J., Musat N., Vagner T. and Kuypers M. M. M. (2012) Look@NanoSIMS - a tool for the analysis of nanoSIMS data in environmental microbiology. *Environ. Microbiol.* **14**, 1009–1023.

Ren H., Brunelle B. G., Sigman D. M. and Robinson R. S. (2013) Diagenetic aluminum uptake into diatom frustules and the preservation of diatom-bound organic nitrogen. *Mar. Chem.* **155**, 92–101.

Rickert D., Schlüter M. and Wallmann K. (2002) Dissolution kinetics of biogenic silica from the water column to the sediments. *Geochim. Cosmochim. Acta* **66**, 439–455.

Rohling E. and Cooke S. (1999) Stable oxygen and carbon isotopes in foraminiferal carbonate shells. In *Modern Foraminifera* (ed. B. Sen Gupta). Kluwer, Dordrecht, pp. 239–258.

Ryves D. B., Leng M. J., Barker P. A., Snelling A. M., Sloane H. J., Arrowsmith C., Tyler J. J., Scott D. R., Radbourne A. D. and Anderson N. J. (2020) Understanding the transfer of contemporary temperature signals into lake sediments via paired oxygen isotope ratios in carbonates and diatom silica: Problems and potential. *Chem. Geol.* **552**, 119705.

Schmidt M., Botz R., Rickert D., Bohrmann G., Hall S. R. and Mann S. (2001) Oxygen isotopes of marine diatoms and relations to opal-A maturation. *Geochim. Cosmochim. Acta* **65**, 201–211.

Shemesh A., Charles C. D. and Fairbanks R. G. (1992) Oxygen isotopes in biogenic silica: global changes in ocean temperature and isotopic composition. *Science* **256**, 1434–1436.

Smith A. C., Leng M. J., Swann G. E. A., Barker P. A., Mackay A. W., Ryves D. B., Sloane H. J., Chenery S. R. N. and Hems M. (2016) An experiment to assess the effects of diatom dissolution on oxygen isotope ratios. *Rapid Commun. Mass Spectrom.* **30**, 293–300.

Swann G. E. A. and Leng M. J. (2009) A review of diatom δ18O in palaeoceanography. *Quat. Sci. Rev.* **28**, 384–398.

Tyler J. J., Sloane H. J., Rickaby R. E. M., Cox E. J. and Leng M. J. (2017) Post-mortem oxygen isotope exchange within cultured diatom silica. *Rapid Commun. Mass Spectrom.* **31**, 1749–1760.

Van Bennekom A. J., Buma A. G. J. and Nolting R. F. (1991) Dissolved aluminium in the Weddell-Scotia Confluence and effect of Al on the dissolution kinetics of biogenic silica. *Mar. Chem.* **35**, 423–434.

Van Cappellen P. and Qiu L. (1997) Biogenic silica dissolution in sediments of the Southern Ocean: II. Kinetics. *Deep. Res. Part II Top. Stud. Oceanogr.* **44**, 1129–1149.

Van Cappellen Philipp, Suvavis Dixi and van Beusekom Justu (2002) Biogenic silica dissolution in the oceans: Reconciling experimental and field-based dissolution rates. *Global Biogeochemical Cycles* **16**(4), 23-1–23-10, In press.

Zachos J. C., Pagani M., Sloan L., Thomas E. and Billups K. (2001) Trends, rhythms, and aberrations in global climate 65 Ma to present. *Science* **292**, 686–693.

Zhuravlev L. T. (2000) The surface chemistry of amorphous silica. Zhuravlev model. *Colloids Surfaces A Physicochem. Eng. Asp.* **173**, 1–38.

*Associate editor:* Hao-Jia Ren